

**Supplementary Information for**  
**High-Stability Electrocatalytic CO<sub>2</sub> Reduction in Seawater**  
**Over Heterostructure Cu-Bi Nanosheets with H-Spillover**  
**Effect**

*Bangli Feng<sup>a,†</sup>, Yixin Ouyang<sup>d,†</sup>, Peng Liu<sup>a</sup>, Shanshan Zheng<sup>a</sup>, Liwen Wang<sup>b</sup>, Yifan Yang<sup>b</sup>, Zisen Wang<sup>b</sup>, Zhifeng Xin,<sup>a,\*</sup> Xiuyun Zhang,<sup>c,\*</sup> Yifa Chen,<sup>b,\*</sup>*

<sup>a</sup>Institute of Molecular Engineering and Applied Chemistry, Anhui University of Technology, Ma'anshan, Anhui 243002, P. R. China.

<sup>b</sup>Guangdong Provincial Key Laboratory of Carbon Dioxide Resource Utilization, School of Chemistry, South China Normal University, Guangzhou, 510006, P. R. China.

<sup>c</sup>College of Physics Science and Technology, Yangzhou University, Yangzhou 225002, China.

<sup>d</sup>State Key Laboratory of Flexible Electronics & Institute of Advanced Materials (IAM), Jiangsu National Synergistic Innovation Center for Advanced Materials (SICAM), Nanjing University of Posts & Telecommunications, Nanjing 210023, China.

<sup>†</sup>Bangli Feng and Yixin Ouyang contributed equally to this work.

\*Correspondence and requests for materials should be addressed to Z. X. ([xinzf521@ahut.edu.cn](mailto:xinzf521@ahut.edu.cn)), X. Z. (email: [xyzhang@yzu.edu.cn](mailto:xyzhang@yzu.edu.cn)), Y. C. (email: [chyf927821@163.com](mailto:chyf927821@163.com)).

## Contents

**Figure S1.** Characterization of BMO NSs. (a) SEM image. (b) TEM image. (c) HRTEM image. (d) STEM image and elemental mapping images.

**Figure S2.** AFM images of Cu/BMO NSs. (a) AMF image. (b) 3D mode image.

**Figure S3.** FTIR spectra of BMO NSs and Cu/BMO NSs.

**Figure S4.** EPR spectra of BMO NSs and Cu/BMO NSs under vacuum and CO<sub>2</sub> atmospheres ( $g = 2.003$ ).

**Figure S5.** XPS spectra of BMO NSs and Cu/BMO NSs.

**Figure S6.** High resolution XPS spectra of Cu/BMO NSs and BMO NSs. (a) Mo 3d. (b) Bi 4f. (c) O 1s. (d) Cu 2p.

**Figure S7.** Collection of natural seawater.

**Figure S8.** CV curves of comparisons at different scanning rates ( $40 \sim 140 \text{ mV S}^{-1}$ ). (a) Cu NPs (b) BMO NSs. (c) Cu/BMO NSs.

**Figure S9.** Characterization of the liquid product. (a) Ion chromatogram. (b) <sup>1</sup>H-NMR spectra.

**Figure S10.** FE of different products for Cu/BMO NSs in 0.1 M KHCO<sub>3</sub>.

**Figure S11.** EDS images of Cu/BMO NSs with different Cu NPs loadings. (a) Cu/BMO NSs (4.14%). (b) Cu/BMO NSs (8.39%). (c) Cu/BMO NSs (1.48%).

**Figure S12.** FE<sub>HCOOH</sub> of Cu/BMO NSs with different content of Cu NPs.

**Figure S13.** FE of different products for Cu/BMO NSs in simulated seawater.

**Figure S14.** Electrochemical properties of Cu/BMO NSs in simulated seawater. (a) LSVs. (b)  $j_{\text{HCOOH}}$  at different potentials.

**Figure S15.** Durability test for Cu/BMO NSs in simulated seawater (0.6 M NaCl) at -0.8 V vs. RHE.

**Figure S16.** Energy efficiency of Cu/BMO NSs at different potentials in simulated seawater.

**Figure S17.** SEM and PXRD tests of Cu/BMO NSs before and after electrocatalysis in simulated seawater. (a) SEM image. (b) PXRD patterns.

**Figure S18.** The pH value and conductivity of cathode and anode electrolytes at the beginning and after the electrocatalysis tests in simulated seawater.

**Figure S19.** FE of different products for Cu/BMO NSs in natural seawater.

**Figure S20.** Electrochemical properties of Cu/BMO NSs in natural seawater. (a) LSVs. (b)  $j_{\text{HCOOH}}$  at different potentials.

**Figure S21.** LSV of Cu/BMO NSs in different electrolytes (simulated seawater, seawater and 0.1 M KHCO<sub>3</sub>).

**Figure S22.** Energy efficiency of Cu/BMO NSs in seawater.

**Figure S23.** SEM and elemental mapping images of Cu/BMO NSs electrode surface after electrocatalysis in natural seawater.

**Figure S24.** The pH value and conductivity of cathode and anode electrolytes at the beginning and after the electrocatalysis tests in natural seawater.

**Figure S24.** Free energy diagrams of the CO<sub>2</sub> reduction pathway toward HCOOH on Bi-O surface (a) and (b) the O-vacancy surface.

**Figure S25.** FE<sub>HCOOH</sub> for Cu/BMO NSs at different potentials in seawater with different pH.

**Figure S26.** Free energy diagrams of the CO<sub>2</sub> reduction pathway toward HCOOH on Bi-O surface (a) O-vacancy surface and (b) the O-vacancy surface.

**Figure S27.** Calculated CO<sub>2</sub> adsorption energy on different sites.

**Figure S28.** Free energy profile of the CO<sub>2</sub> reduction pathway toward CO on the Cu/BMO NSs.

## **2. Supplementary Table**

**Table S1.** The summary of CO<sub>2</sub> electro-reduction performances of Cu/BMO NSs and other electrocatalysts in H-type cells.

**Table S2.** The summary of CO<sub>2</sub> electro-reduction performances of Cu/BMO NSs and other electrocatalysts in seawater.

**Table S3.** The metal ions concentration in seawater before and after electrocatalysis for 10 h measured by ICP-MS.

## Experimental section

### Materials

All chemicals and solvents were commercially available and used without further purification. Hexadecyltrimethylammonium bromide (CTAB),  $\text{Na}_2\text{MnO}_4 \cdot 2\text{H}_2\text{O}$ ,  $\text{Bi}(\text{NO}_3)_3 \cdot 5\text{H}_2\text{O}$ , Trisodium citrate dihydrate and  $\text{NaBH}_4$  are purchased from Sinopharm Chemical Reagent Co., Ltd.  $\text{Cu}(\text{NO}_3)_2 \cdot 3\text{H}_2\text{O}$  is purchased from Shanghai Taitan Scientific Co., Ltd. All aqueous solutions are prepared with Millipore water (18.25 M $\Omega$ ).

### Experimental Section

*Preparation of BMO:* 30 mL  $\text{Na}_2\text{MoO}_4 \cdot 2\text{H}_2\text{O}$  (0.18 g, 0.75 mmol) deionized water solution and 30 mL  $\text{Bi}(\text{NO}_3)_3 \cdot 5\text{H}_2\text{O}$  (0.73 g, 1.50 mmol) ethylene glycol solution was mixed and stirred until dissolved, and then CTAB (0.36 g, 1.00 mmol) was added to the above mixture and stirred for 20 minutes. Then, the mixture was transferred into a polytetrafluoroethylene lined reactor, sealed and heated at 120 °C for 24 h. The solution was centrifuged, washed with water and ethanol for several times, and then placed in an oven to dry at 60 °C overnight to obtain the product.

*Preparation for BMO NSs:* 200 mg BMO was dissolved in 30 mL water and the resulting dispersion was sonicated at 200 W for 3 h. The solution was centrifuged, washed with water and ethanol for several times, and then placed in an oven to dry at 60 °C overnight to obtain the product.

*Synthesis of Cu/BMO NSs:* 200 mg BMO was dissolved in 30 mL water and the resulting dispersion was sonicated at high frequency for 3 h to generate the BMO NSs dispersion. Then,  $\text{Cu}(\text{NO}_3)_2 \cdot 3\text{H}_2\text{O}$  (0.06 g, 0.25 mmol) and trisodium citrate dihydrate (0.15 g, 0.50 mmol) were added in 10 mL 0.1 M HCl solution, dissolved and added into the dispersion of BMO NSs, and stirred at 45 °C for 6 h in a water bath. Then, 1 mL  $\text{NaBH}_4$  (0.076g, 2 mmol) solution was slowly added to the above suspension and stirred in an ice bath for 2 h. Finally, the mixture was centrifuged, washed several times with deionized water and acetone, and dried in a vacuum drying oven at 60 °C for 10 h. In addition, Cu/BMO NSs with different Cu NPs loadings were synthesized by adding different amount of  $\text{Cu}(\text{NO}_3)_2 \cdot 3\text{H}_2\text{O}$  (e.g., 0.15, 0.25, and 0.35 mmol), and the samples

were denoted as Cu/BMO NSs (1.48%, 4.14%, and 8.39%), respectively.

### **Characterizations**

Powder X-ray diffraction (PXRD) experiments are recorded on Bruker D8 Advance (operating at 40 kV and 20 mA) with Ni-filtered Cu K $\alpha$  radiation at 1.5406 (Å) with a speed of 5 min<sup>-1</sup>. SEM images are obtained from a FEI NOVA NANO 430 Field emission scanning electron microscope equipped with an Oxford Energy Dispersive X-ray spectroscopy. X-ray Photoelectron Spectroscopy (XPS) was carried out on a Thermo ESCALAB 250XI multifunctional imaging electron spectrometer using the binding energy of C as the internal standard. TEM images and STEM-HAADF images coupled to EDS elemental mapping were collected on a JEOL JEM-2100 electron microscope at 200 kV equipped with an Oxford Energy Dispersive X-ray spectroscopy. Atomic force microscope (AFM) images were measured on a Shimadzu SPM-Nanoa Atomic Force Microscopy.

### **The preparation of working electrode**

10 mg sample and 10 mg acetylene black were grinded for 10 min and dispersed in 1 mL 0.5% Nafion solution followed with sonication for 30 min to form uniform catalyst ink. The ink was dropped directly on a hydrophobic carbon paper (1 cm  $\times$  2 cm) to form a 1  $\times$  1 cm<sup>2</sup> catalyst area with a catalyst loading of  $\sim$ 1 mg cm<sup>-2</sup> (cathode) and  $\sim$ 2 mg cm<sup>-2</sup> (anode). The deposited carbon paper was further dried at room temperature.

### **Electrocatalytic CO<sub>2</sub>RR tests**

All electrochemical tests were performed in a standard three-electrode configuration in 0.1 M KHCO<sub>3</sub>, simulated seawater (0.6 M NaCl) and natural seawater using a CHI660-E electrochemical workstation. Carbon rod and Ag/AgCl were used as counter electrode and reference electrode, respectively, and modified carbon paper (1 cm  $\times$  1 cm) is used as work electrode. The electro-chemical CO<sub>2</sub>RR performance was

carried out in an airtight electro-chemical H-type cell, in which, two compartments were separated by a Nafion®117 proton exchange membrane to prevent mixing of products from the two electrode chambers. The polarization curves were performed by linear sweep voltammetry (LSV) mode at a scan rate of 5 mV s<sup>-1</sup>. In this experiment, polarization curves were recorded successively in Ar-saturated and CO<sub>2</sub> saturated KHCO<sub>3</sub> solution. The measurement of electrochemical impedance spectroscopy (EIS) was carried out under the open circuit voltage. During the measurement process, 10 mV amplitude AC voltage was applied in the frequency range of 1000 kHz to 100 MHz. To estimate the electrochemical active surface area (ECSA), cyclic voltammograms (CV) were tested under the potential window of -0.1 V ~ 0 V (vs. Ag/AgCl) with various scan rates from 20 to 100 mV s<sup>-1</sup>. In this work, all the potentials were measured vs. Ag/AgCl electrode, and the results were calculated to the potential vs. reversible hydrogen electrode (RHE) based on the Nernst equation: E (vs. RHE) = E (vs. Ag/AgCl) + 0.1989 V + 0.059 × pH (without iR compensation).

The gaseous reduction products were monitored by a gas chromatography (Shimadzu-2010 plus) equipped with a flame ionization detector (FID) and a thermal conductivity detector (TCD). The liquid products (e.g., formate) were collected from the anode chambers after electrolysis and detected by NMR and ion chromatography. In this work, all reported values were average ones calculated from three or more independent measurements, and all errors were given as standard deviations.

### **Evaluation of CO<sub>2</sub>RR performance**

For products, Faradaic efficiency (FE<sub>CO</sub>) was calculated according to the following equation:

For HCOOH

$$FE_{HCOOH} = \frac{2 \times F \times n_{HCOOH}}{Q} \times 100\%$$

For CO

$$FE_{CO} = \frac{2 \times F \times n_{CO}}{Q} \times 100\%$$

For H<sub>2</sub>

$$FE_{H_2} = \frac{2 \times F \times n_{H_2}}{Q} \times 100\%$$

N: the number of electrons transferred for product formation.

F: Faraday constant, 96485 C mol<sup>-1</sup>.

$n_{products}$  : the moles of products.

Q: the total charge obtained from chronoamperometry (C).

The calculation of energy efficiency (EE, %)

$$EE (\%) = \frac{E_j^0 \times FE_j}{E_j^0 + \eta} \times 100\%$$

$E_j^0$ : the equilibrium cell potential for a certain product (V).

FE<sub>j</sub>: the Faradaic efficiency of the aiming product j (%).

$\eta$  : the overpotential (V).

Reaction rate of the catalysts ( $r$ , mol h<sup>-1</sup> m<sup>-2</sup>):

$$r = \frac{j \times FE}{n \times F}$$

j: total current density.

n: the number of transferred electrons.

F: Faradaic constant (96485 C mol<sup>-1</sup>).

### Computational details

Density functional theory (DFT) calculations were conducted using the Vienna Ab Initio Simulation Package<sup>1</sup> with the Perdew-Burke-Ernzerhof<sup>1, 2</sup> exchange-correlation functional. During structural optimization, convergence criteria were set at 10<sup>-4</sup> eV for total energy and 0.02 eV Å<sup>-1</sup> for atomic forces. A plane-wave cutoff energy of 400 eV was employed. Van der Waals interactions were incorporated using the DFT-D3 dispersion correction method.<sup>4</sup> The binding energies of CO<sub>2</sub> and hydrogen were defined as  $\Delta E_{CO_2} = E_{Catal+CO_2} - E_{Catal} - E_{CO_2}$  and  $\Delta E_H = E_{Catal+H} - E_{Catal} - E_{H_2}/2$ , respectively. Gibbs free

energy changes for elementary reaction steps were determined using the computational hydrogen electrode approach.<sup>3, 4</sup> The Cu/BMO NSs catalyst was modeled with a 4×4 periodic cell featuring a Cu<sub>16</sub> cluster loaded onto a Bi-O terminal slab.

The calculation of Gibbs free energy  $G$  is as follows:

$$G = E_{\text{DFT}} + E_{\text{ZPE}} - TS + \int C_p dT$$

Among them,  $E_{\text{DFT}}$ ,  $E_{\text{ZPE}}$ ,  $T$ ,  $S$  and  $C_p$  are respectively the total energy, zero-point energy, temperature, entropy and heat capacity of the system. The values of  $E_{\text{ZPE}}$ ,  $TS$  and  $\int C_p dT$  can be obtained through frequency calculation:

$$E_{\text{ZPE}} = \frac{1}{2} \sum_i h\nu_i$$

$$-TS = K_B T \sum_i \ln \left( 1 - e^{-\frac{h\nu_i}{K_B T}} \right) - \sum_i h\nu_i \left( \frac{1}{e^{\frac{h\nu_i}{K_B T}} - 1} \right)$$

$$\int C_p dT = \sum_i h\nu_i \left( \frac{1}{e^{\frac{h\nu_i}{K_B T}} - 1} \right)$$

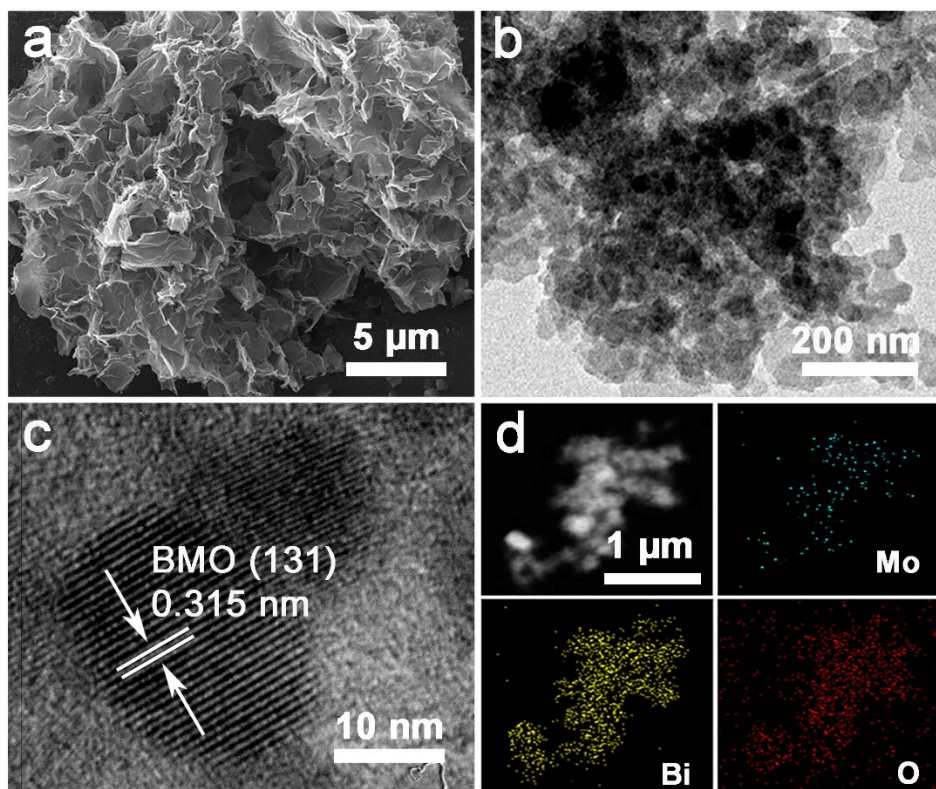


**Figure S1.** Characterization of BMO NSs. (a) SEM image. (b) TEM image. (c) HRTEM image. (d) STEM image and elemental mapping images.

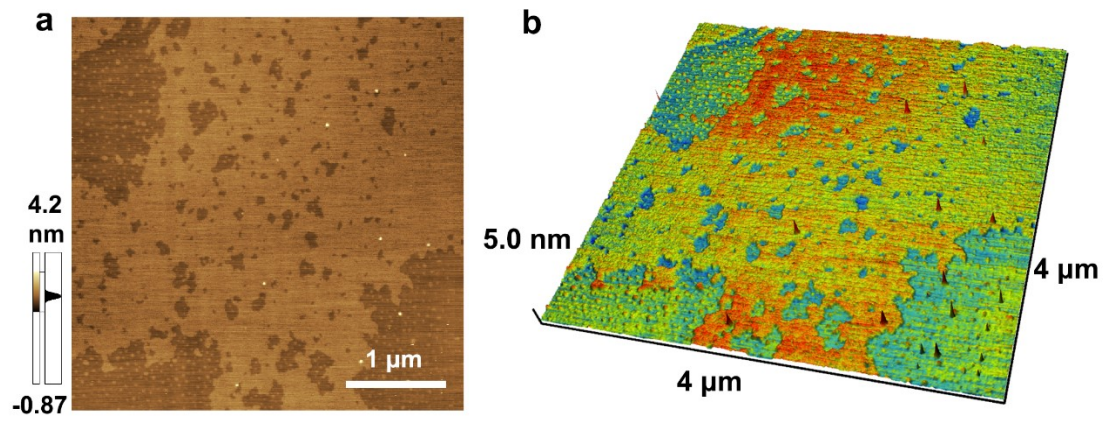


**Figure S2.** AFM images of Cu/BMO NSs. (a) AMF image. (b) 3D mode image.

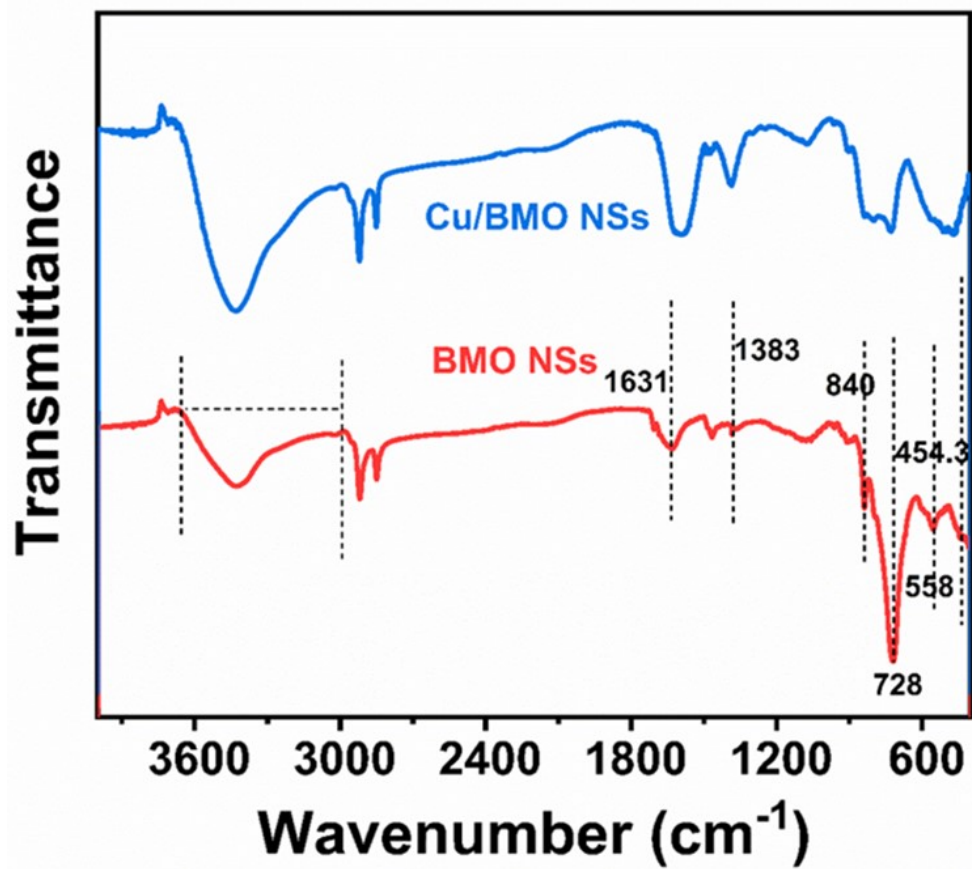
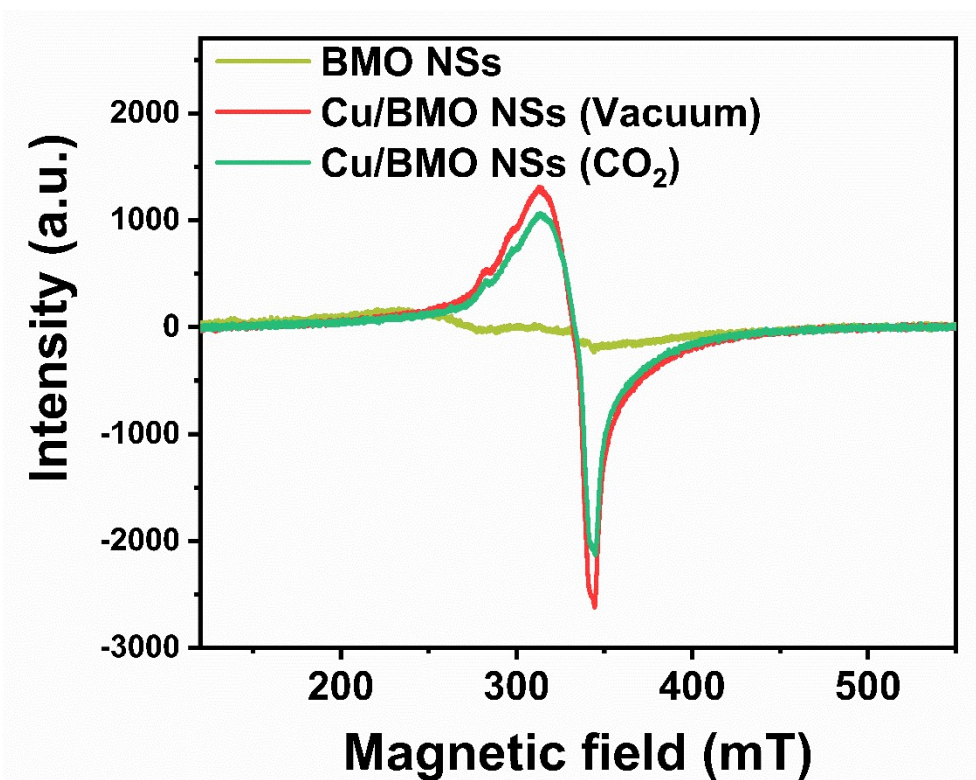


Figure S3. FTIR spectra of BMO NSs and Cu/BMO NSs.



**Figure S4.** EPR spectra of BMO NSs and Cu/BMO NSs under vacuum and CO<sub>2</sub> atmospheres ( $g = 2.003$ ).

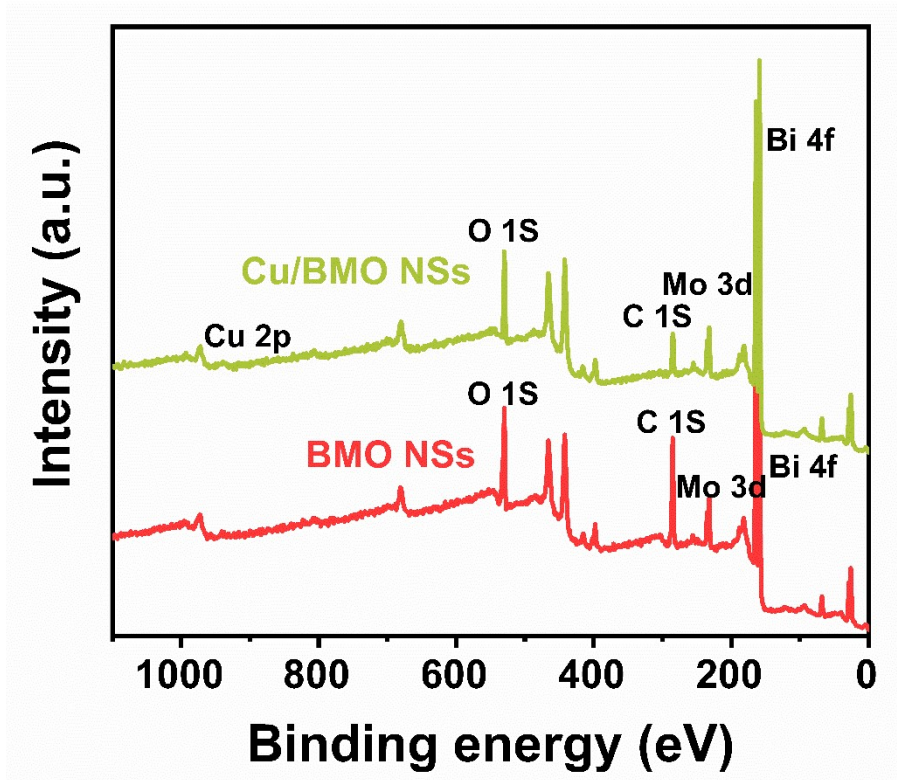
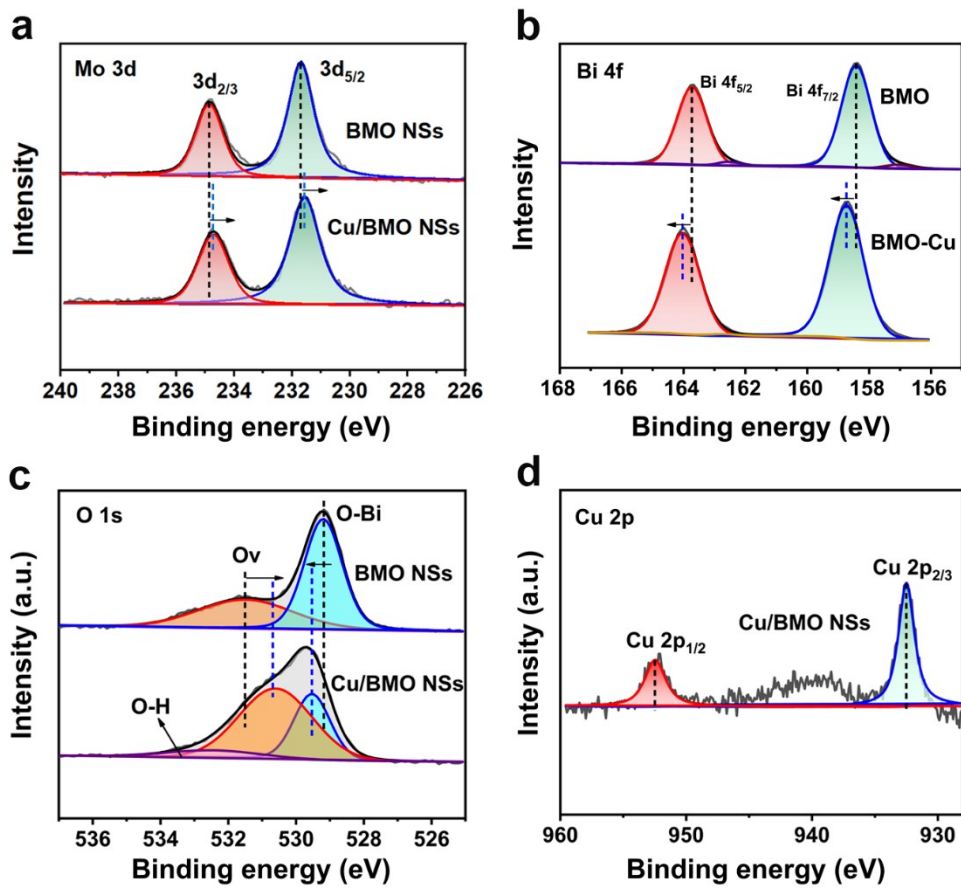
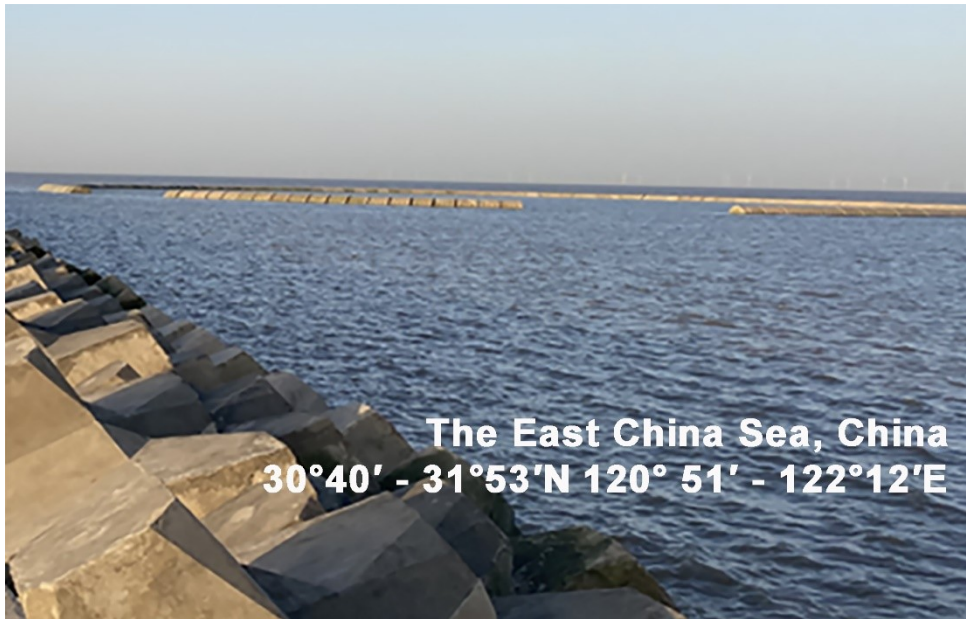


Figure S5. XPS spectra of BMO NSs and Cu/BMO NSs.



**Figure S6.** High resolution XPS spectra of Cu/BMO NSs and BMO NSs. (a) Mo 3d. (b) Bi 4f. (c) O 1s. (d) Cu 2p.



**Figure S7.** Collection of natural seawater (a photo of a seaside in Shanghai, China on May 02, 2024).

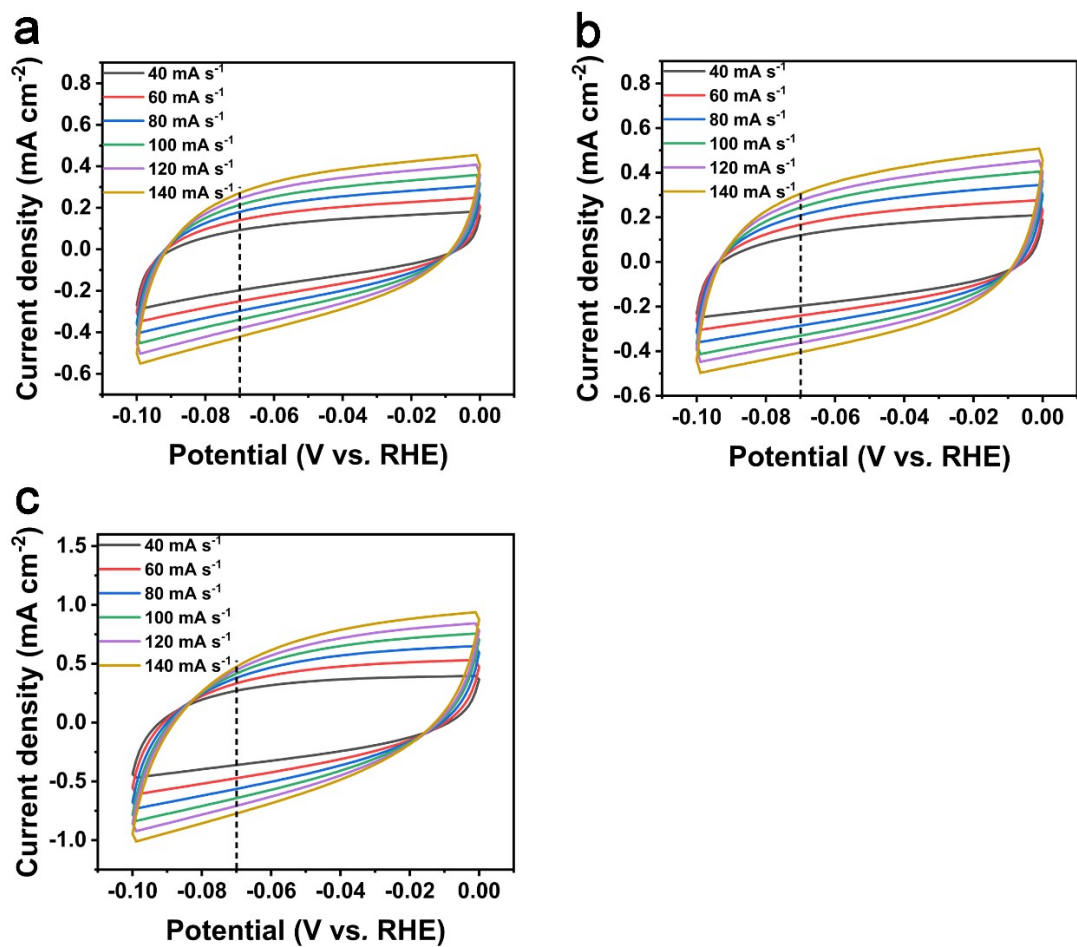


**Figure S8.** CV curves of comparisons at different scanning rates (40 ~ 140 mV S<sup>-1</sup>). (a) Cu NPs (b) BMO NSs. (c) Cu/BMO NSs.

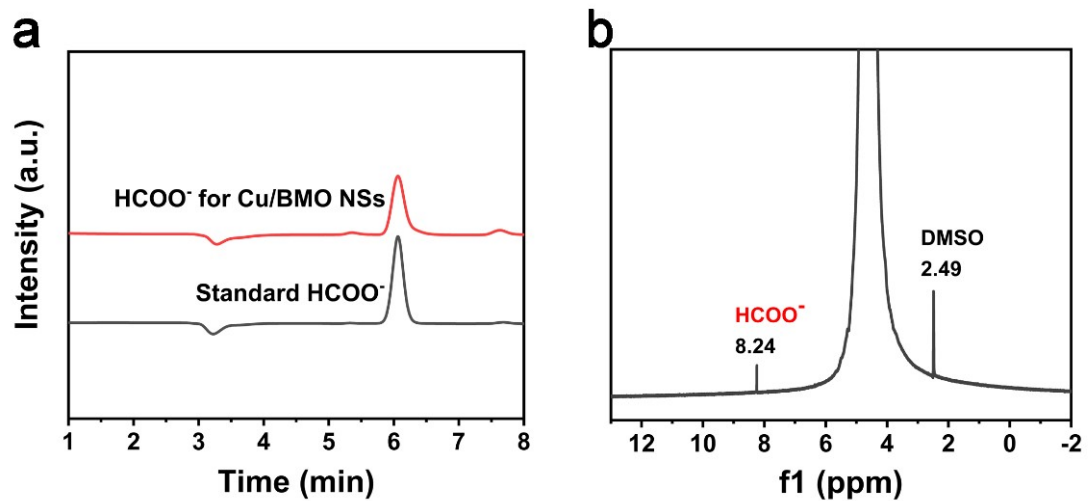


**Figure S9.** Characterization of the liquid product. (a) Ion chromatogram. (b) <sup>1</sup>H-NMR spectra.

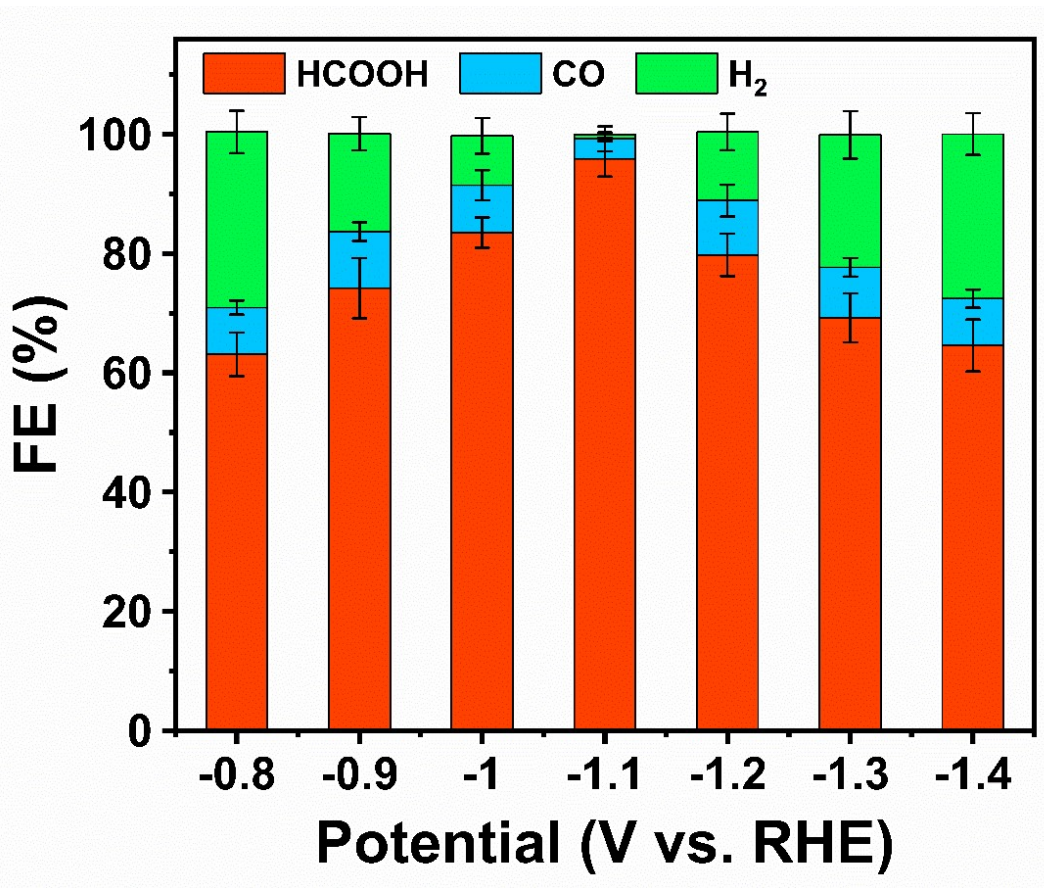
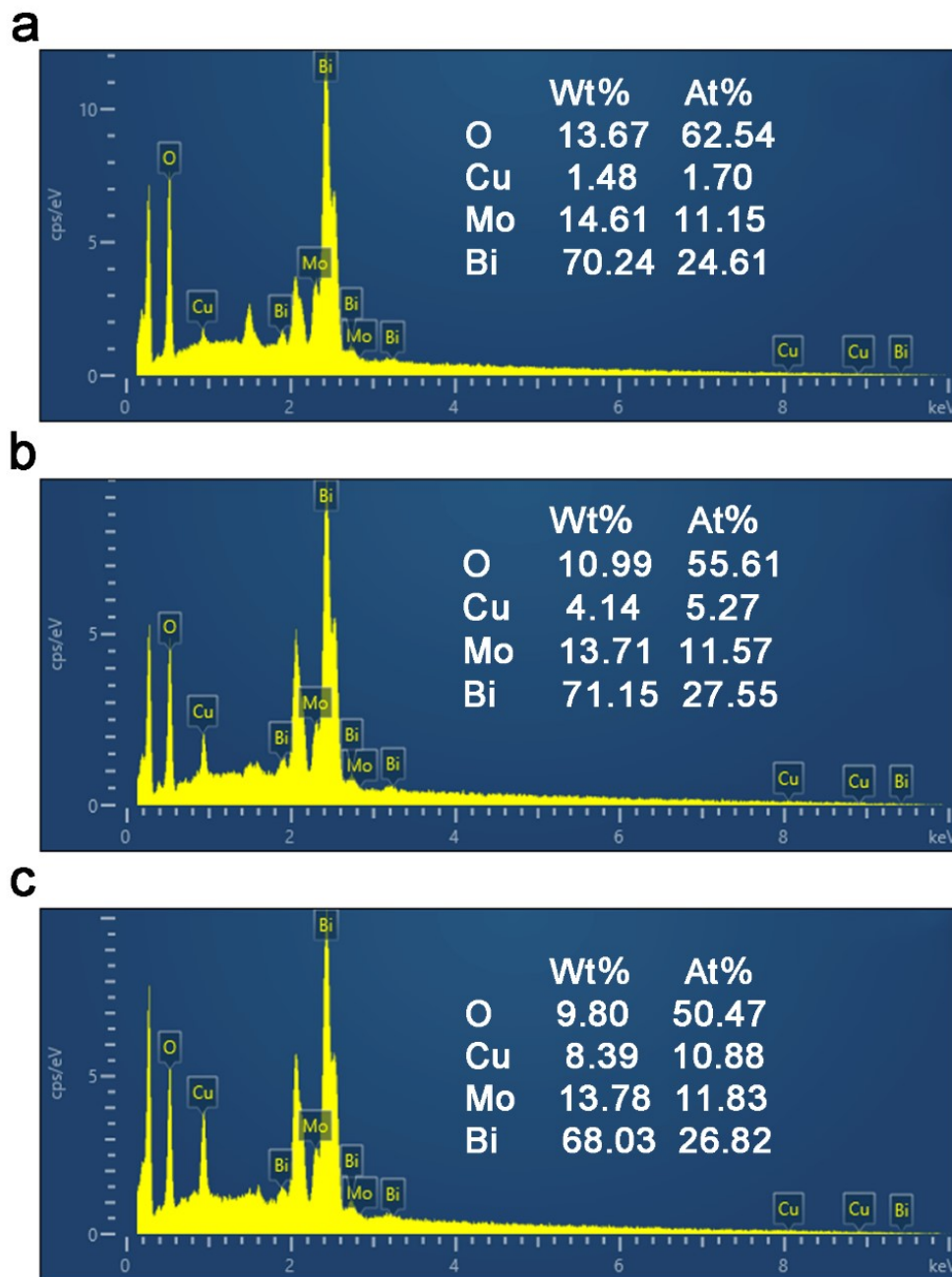


Figure S10. FE of different products for Cu/BMO NSs in 0.1 M KHCO<sub>3</sub>.



**Figure 11.** EDS images of Cu/BMO NSs with different Cu NPs loadings. (a) Cu/BMO NSs (4.14%). (b) Cu/BMO NSs (8.39%). (c) Cu/BMO NSs (1.48%).

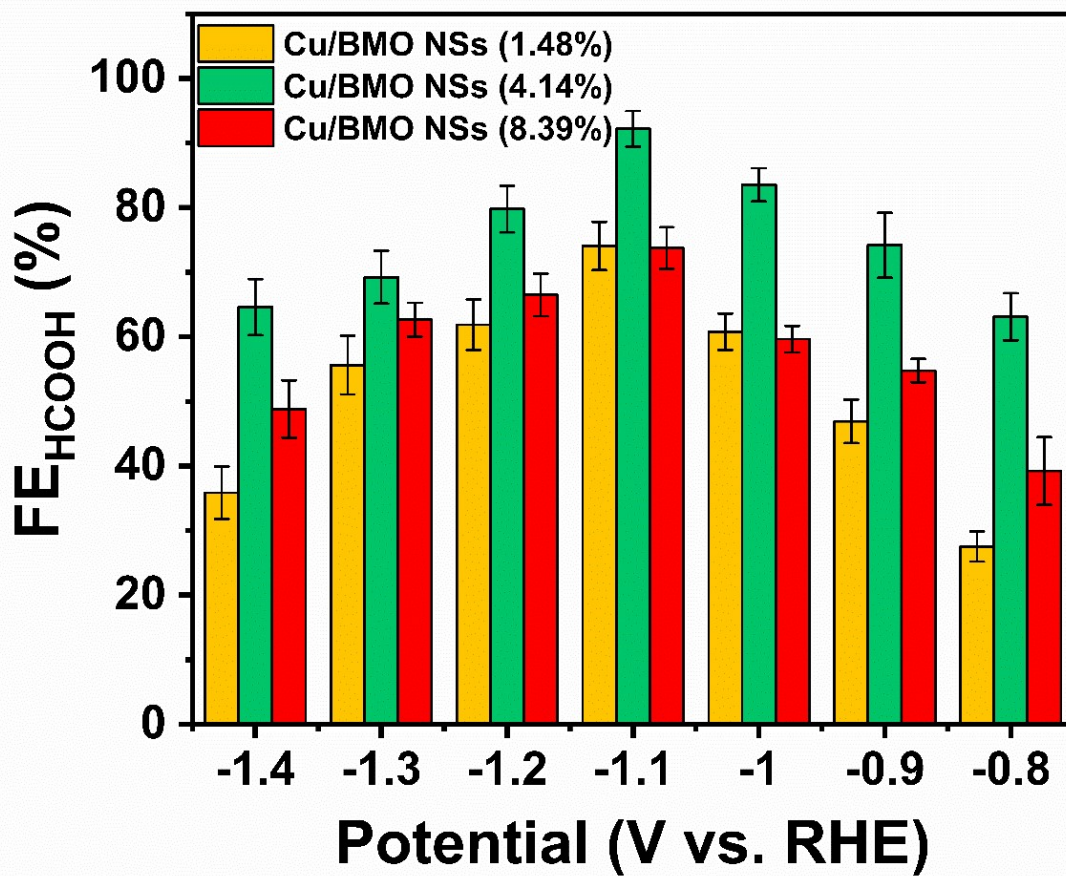


Figure S12. FE<sub>HCOOH</sub> of Cu/BMO NSs with different content of Cu NPs.

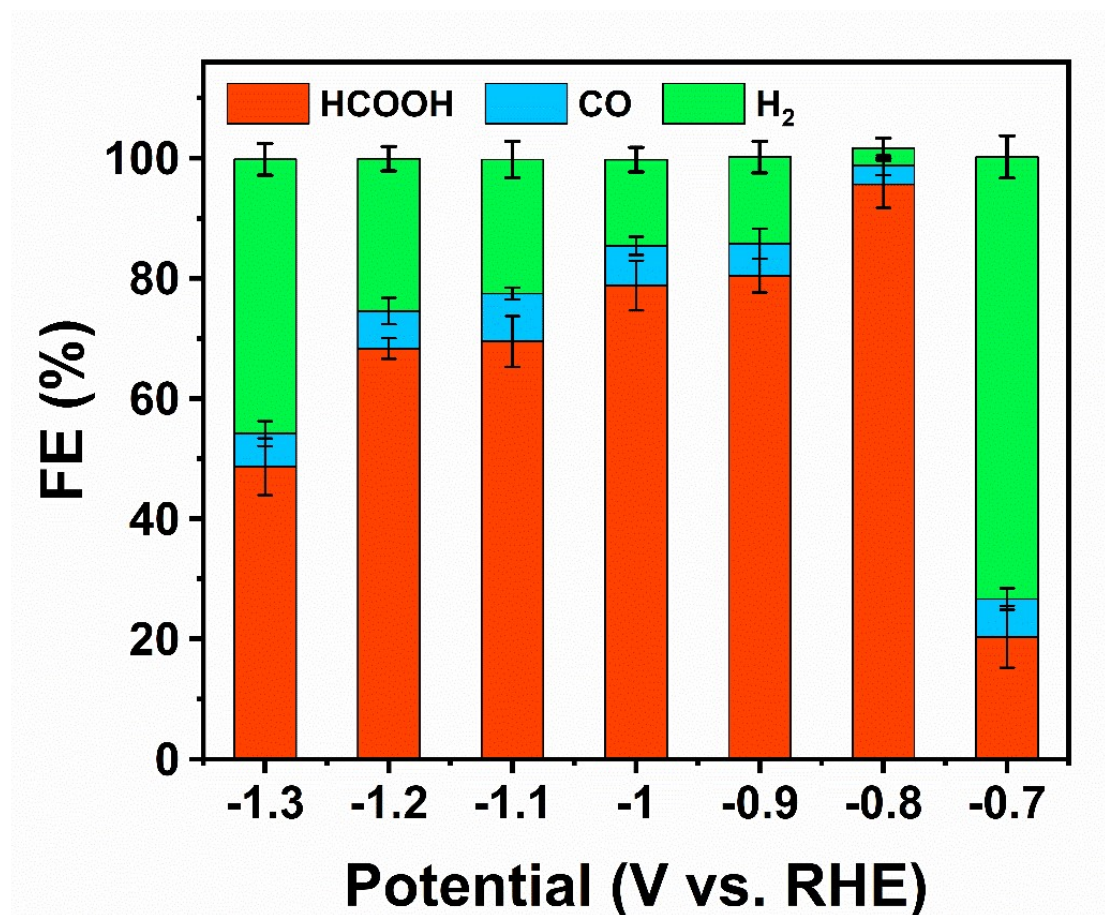
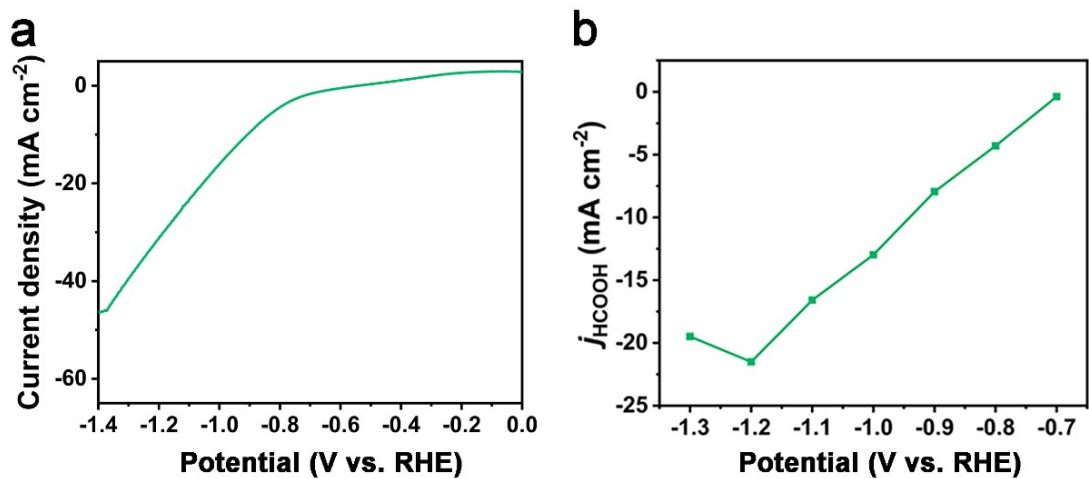
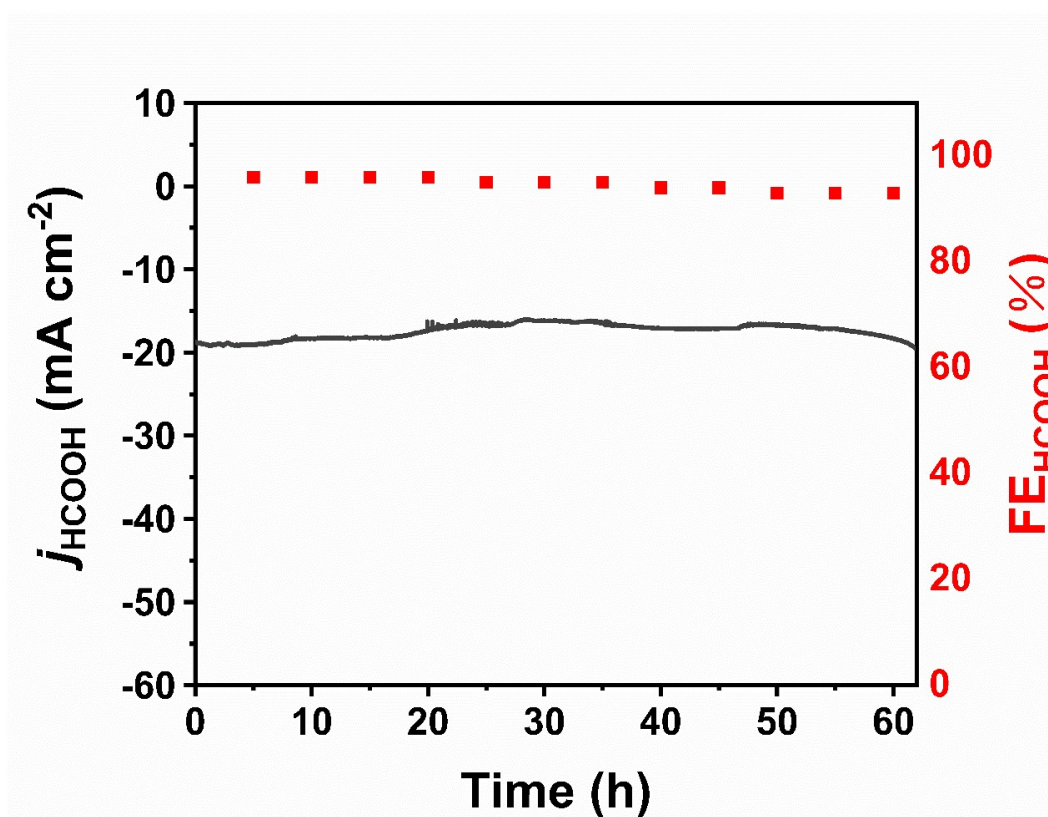


Figure S13. FE of different products for Cu/BMO NSs in simulated seawater.



**Figure S14.** Electrochemical properties of Cu/BMO NSs in simulated seawater. (a) LSVs. (b)  $j_{\text{HCOOH}}$  at different potentials.



**Figure S15.** Durability test for Cu/BMO NSs in simulated seawater (0.6 M NaCl) at -0.8 V vs. RHE.

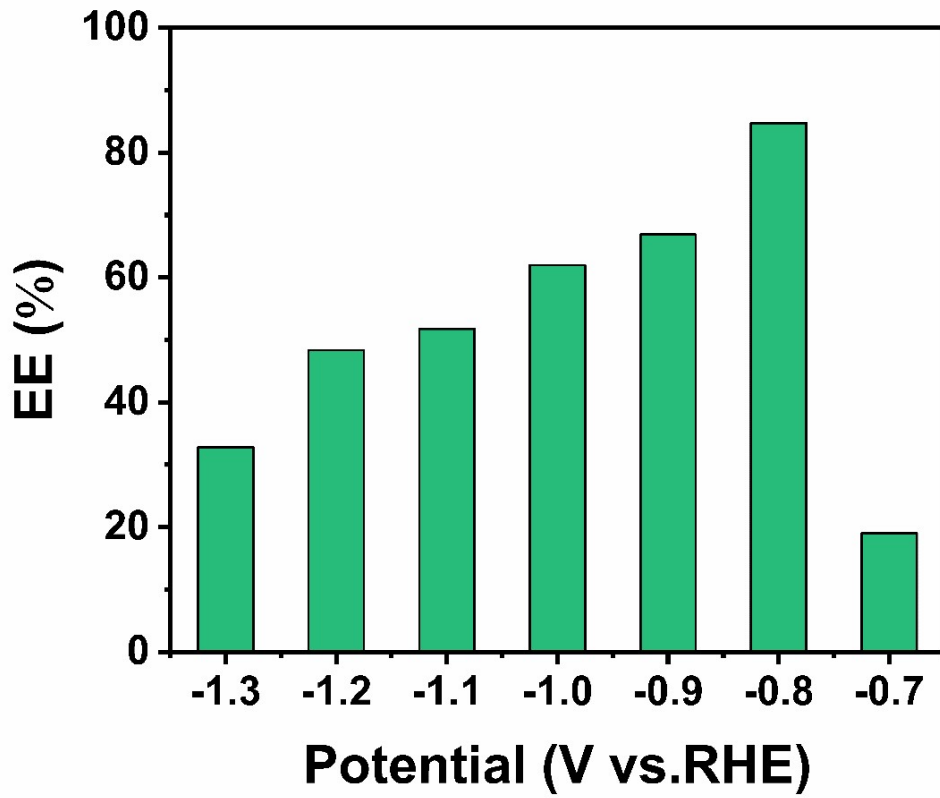


**Figure S16.** Energy efficiency of Cu/BMO NSs at different potentials in simulated seawater.

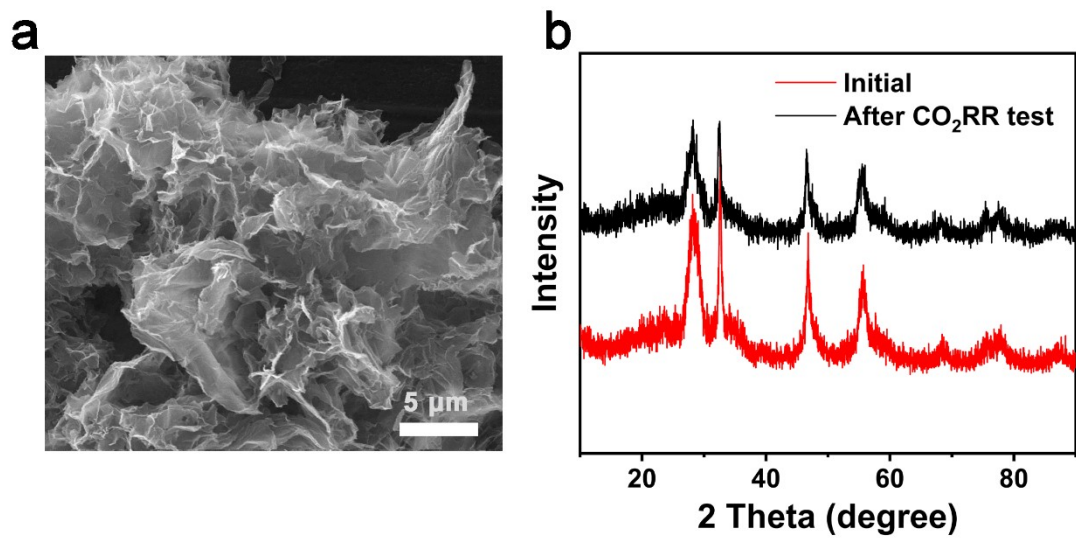


**Figure S17.** SEM and PXRD tests of Cu/BMO NSs before and after electrocatalysis for 10 h in simulated seawater. (a) SEM image. (b) PXRD patterns.

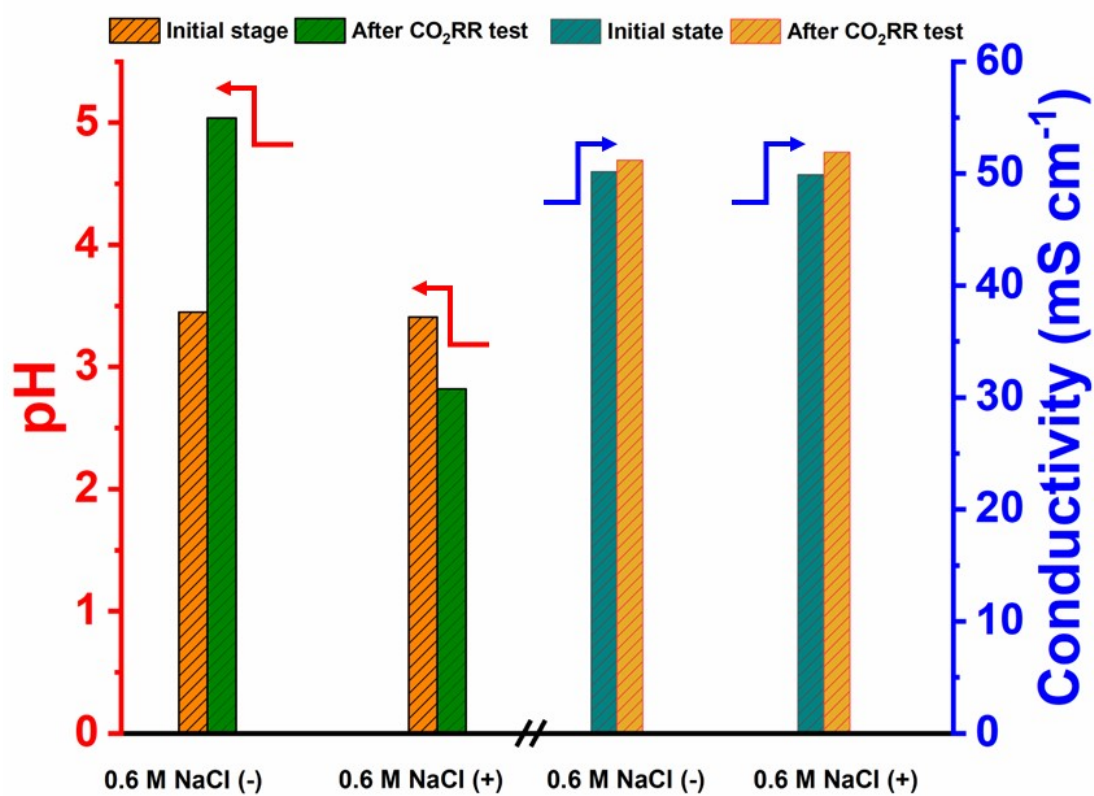


**Figure S18.** The pH value and conductivity of cathode and anode electrolytes at the beginning and after the electrocatalysis tests in simulated seawater.

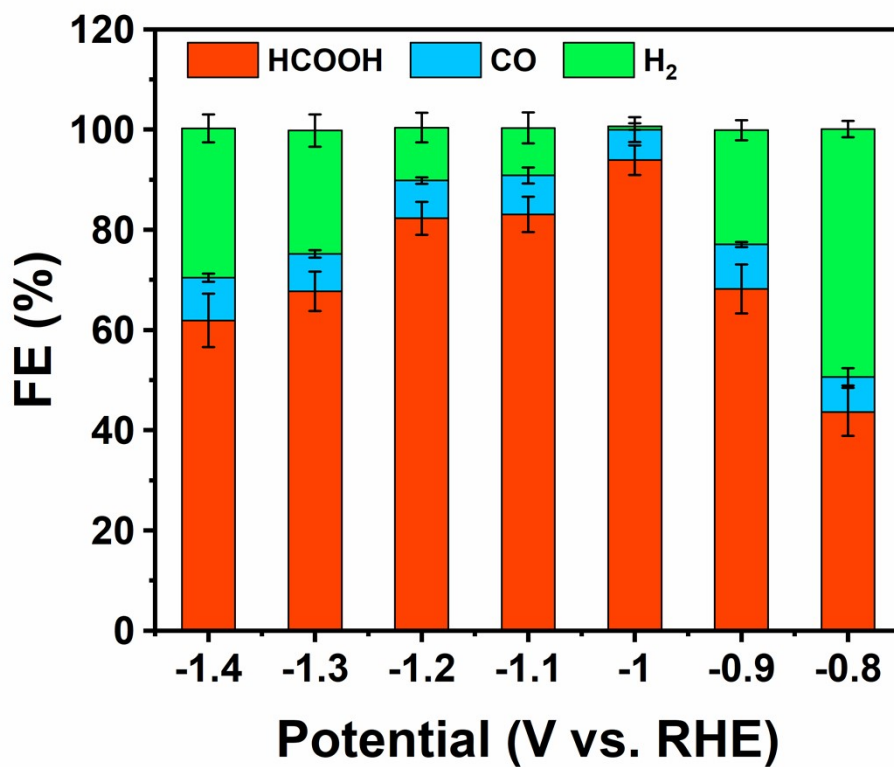
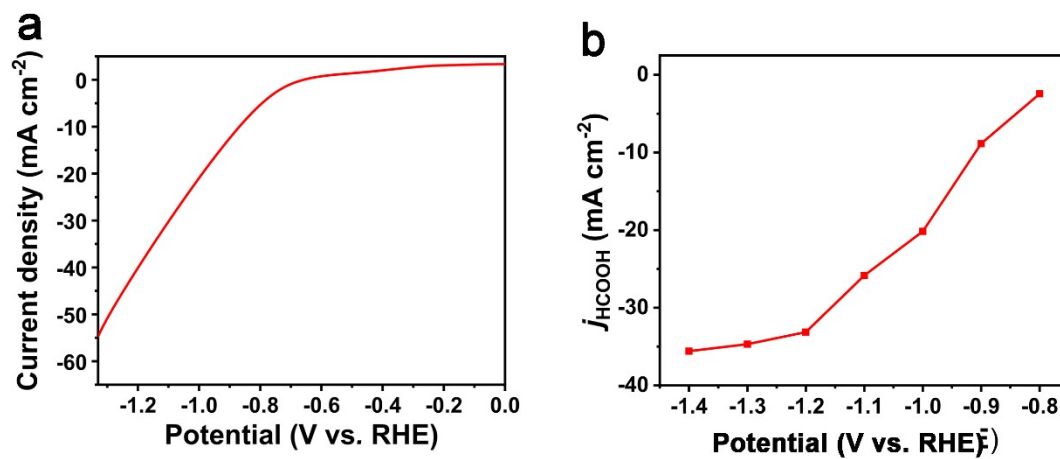
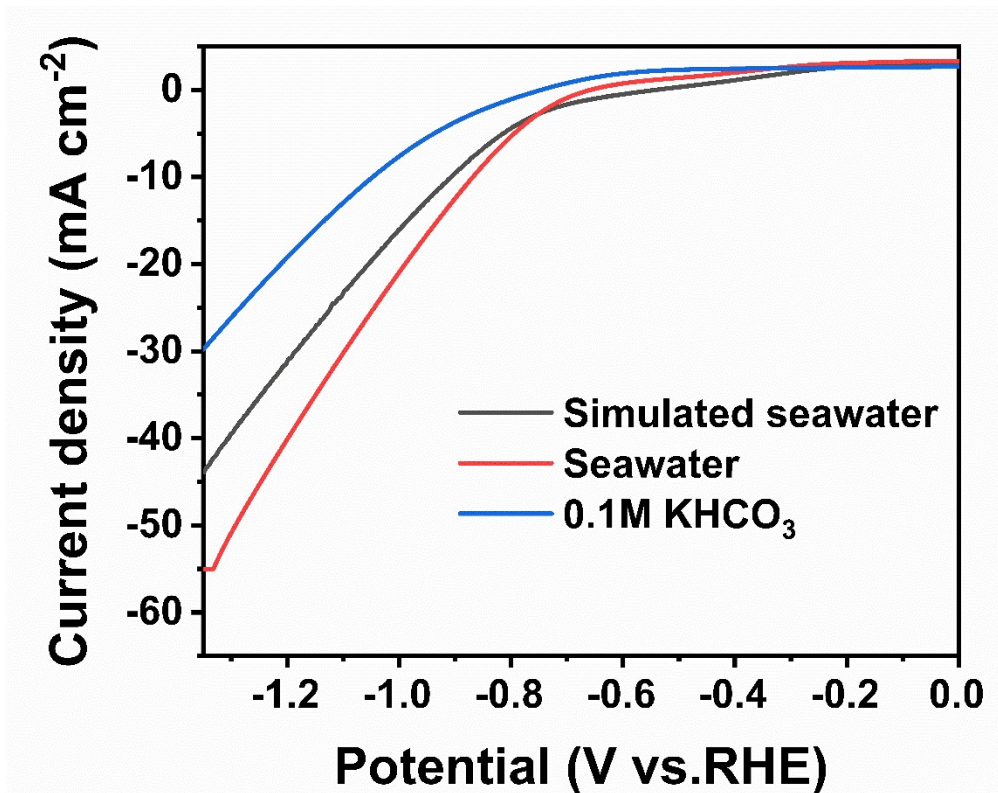


Figure S19. FE of different products for Cu/BMO NSs in natural seawater.



**Figure S20.** Electrochemical properties of Cu/BMO NSs in natural seawater. (a) LSVs. (b)  $j_{\text{HCOOH}}$  at different potentials.



**Figure S21.** LSV of Cu/BMO NSs in different electrolytes (simulated seawater, natural seawater and 0.1 M KHCO<sub>3</sub>).

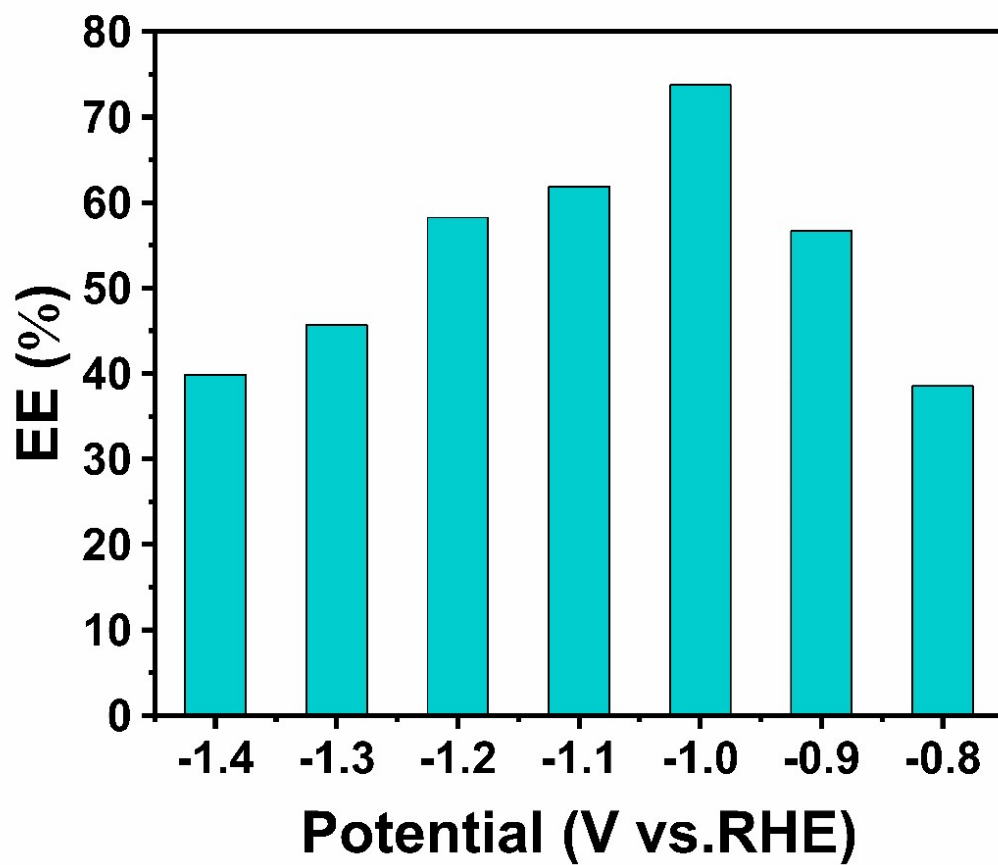
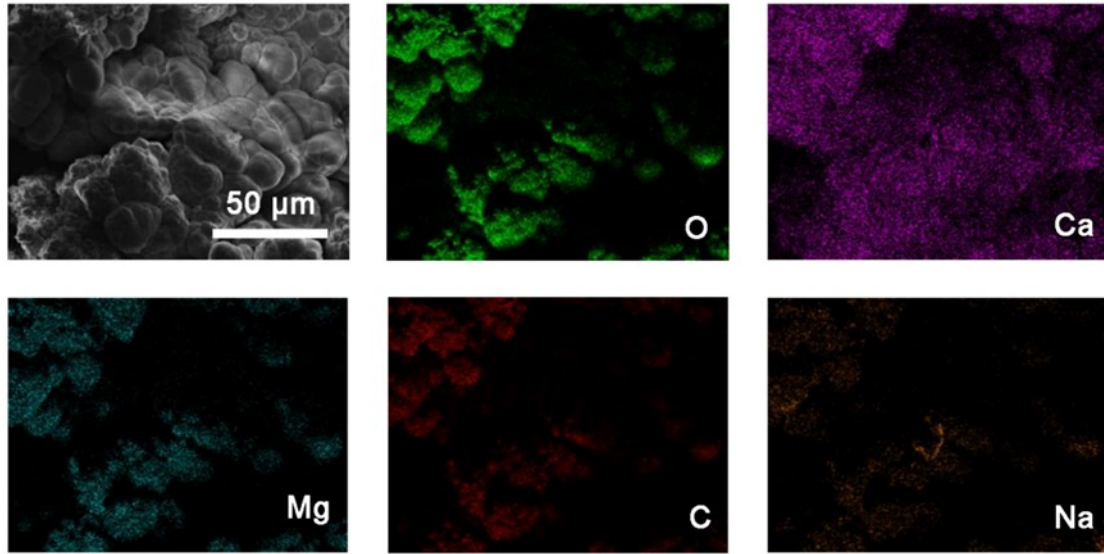
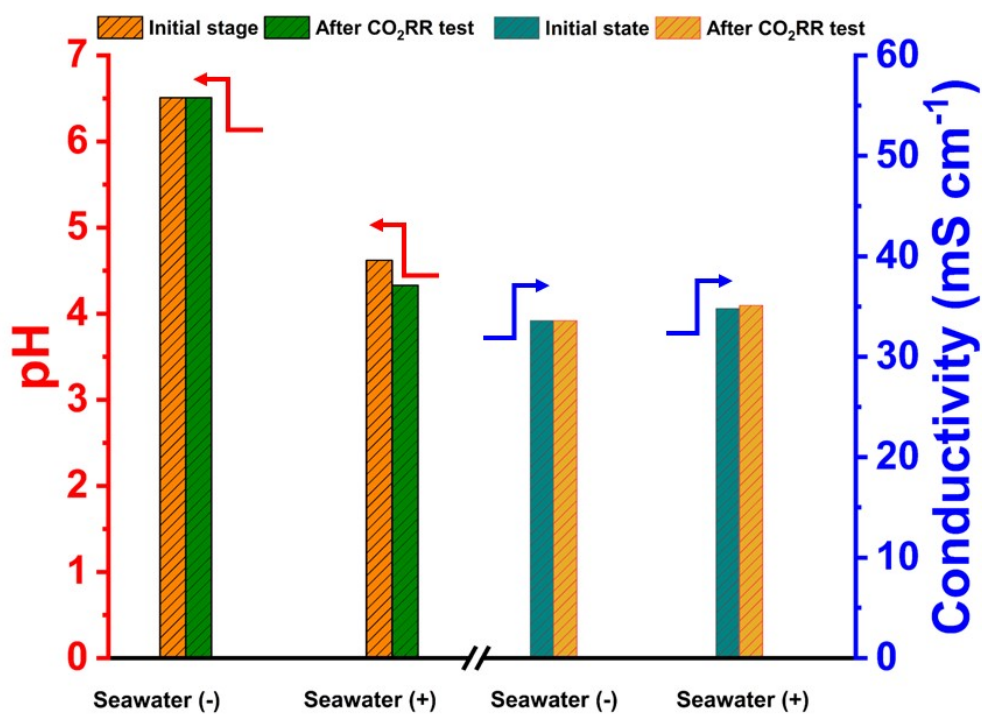


Figure S22. Energy efficiency of Cu/BMO NSs in natural seawater.



**Figure S23.** SEM and elemental mapping images of Cu/BMO NSs electrode surface after electrocatalysis in natural seawater.



**Figure S24.** The pH value and conductivity of cathode and anode electrolytes at the beginning and after the electrocatalysis tests in natural seawater.

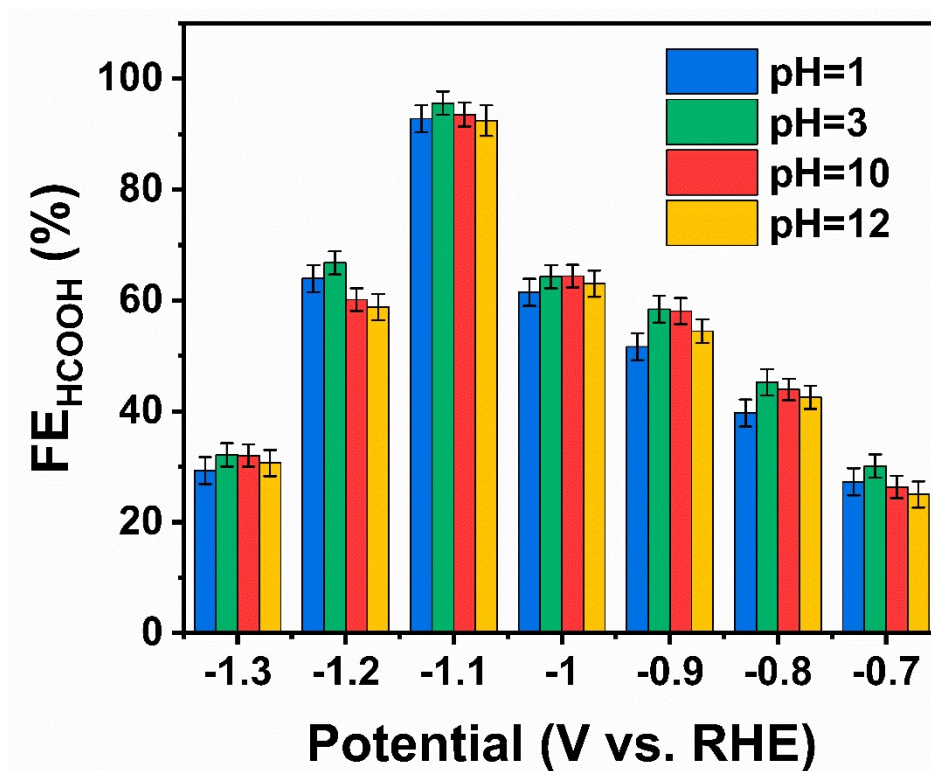


**Figure S25.**  $FE_{HCOOH}$  for Cu/BMO NSs at different potentials in seawater with different pH.

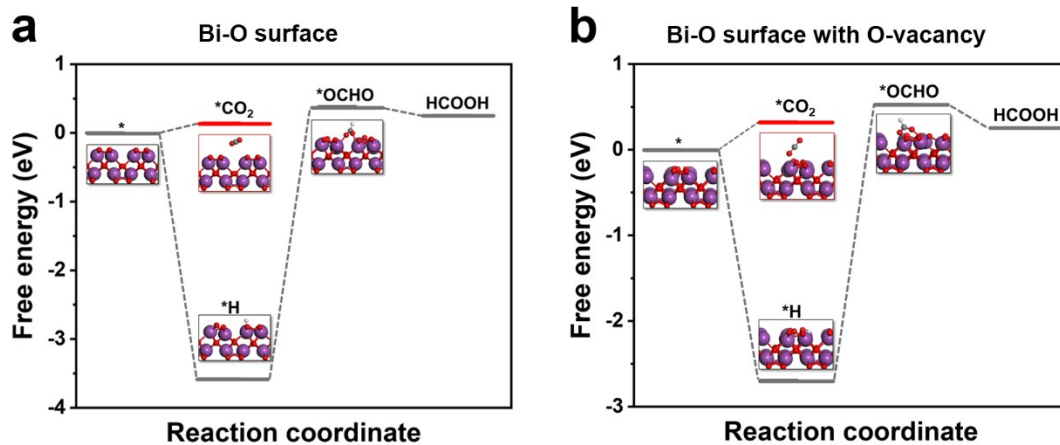


**Figure S26.** Free energy diagrams of the CO<sub>2</sub> reduction pathway toward HCOOH on Bi-O surface (a) O-vacancy surface and (b) the O-vacancy surface.

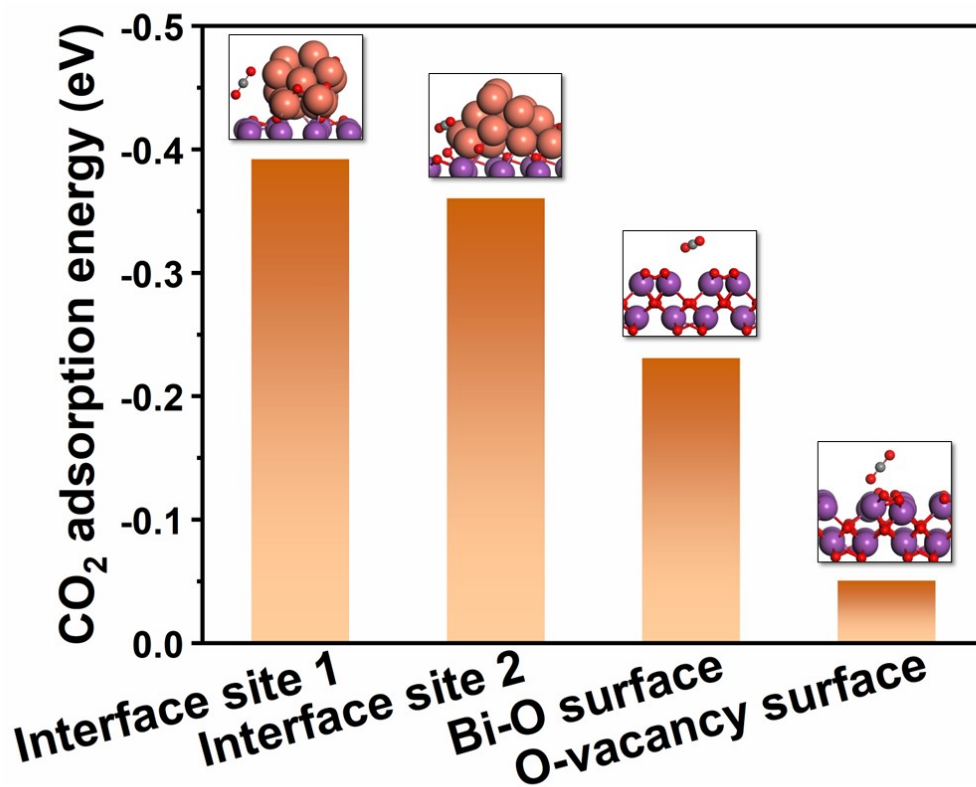
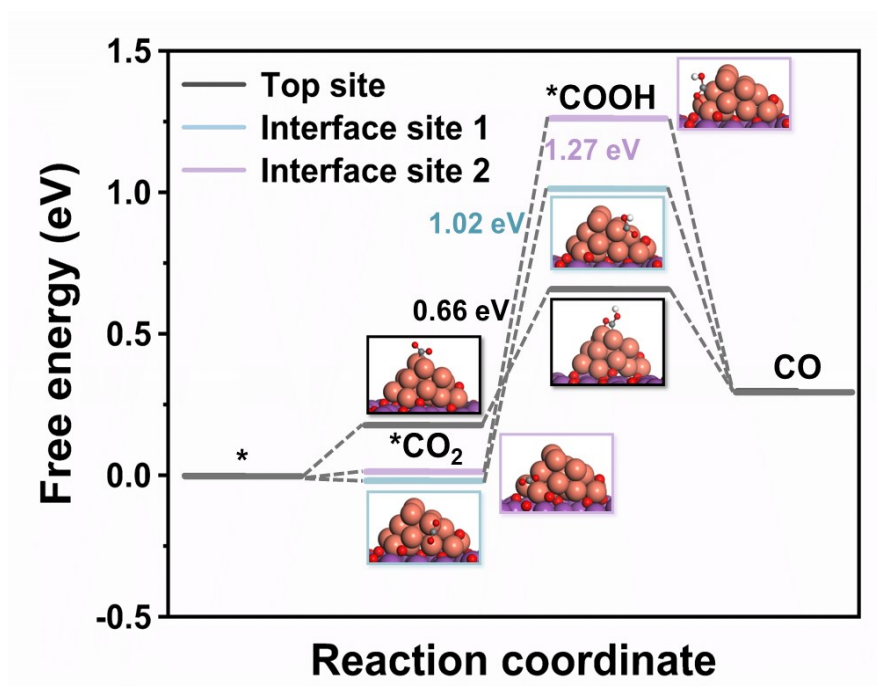


Figure S27. Calculated CO<sub>2</sub> adsorption energy on different sites.



**Figure S28.** Free energy profile of the CO<sub>2</sub> reduction pathway toward CO on the Cu/BMO NSs.

**Table S1.** The summary of CO<sub>2</sub> electro-reduction performances of Cu/BMO NSs and other electrocatalysts in H-type cells.

|          | <b>Catalyst</b>   | <b>FE (%)</b> | <b>j<sub>HCOOH</sub></b><br>(mA cm <sup>-2</sup> ) | <b>Potential</b><br>(V vs. RHE) | <b>r</b><br>(mol m <sup>-2</sup> h <sup>-1</sup> ) | <b>Ref.</b>      |
|----------|---|---------------|--|---------------------------------|--|------------------|
| <b>1</b> | <b>Cu/BMO NSs</b>   | <b>96.00</b>  | <b>35.59</b>                                       | <b>-1.00</b>                    | <b>6.64</b><br><b>(-1.4 V)</b>                     | <b>This work</b> |
| 2        | Cu <sub>0.66</sub> : Bi <sub>0.34</sub>                                 | 98.00         | 6.90   | -0.93                           | 0.91<br>(-0.93 V)                                  | [5]              |
| 3        | Bi/Bi <sub>2</sub> O <sub>2</sub> CO <sub>3</sub>                       | 96.00         | 25.00  | -0.90                           | 4.48<br>(-1.1 V)                                   | [6]              |
| 4        | S-In <sub>2</sub> O <sub>3</sub> /CP                                    | 97.10         | 8.00   | -1.1                            | 1.45<br>(-1.1 V)                                   | [7]              |
| 5        | 10In-SnO <sub>2</sub> /C  | 79.20         | 16.00  | -0.99                           | 2.36<br>(-1.09 V)                                  | [8]              |
| 6        | Bi-Sn   | 93.90         | 12.00  | -1.00                           | 3.02<br>(-1.20 V)                                  | [9]              |
| 7        | SnO <sub>2</sub> /Bi <sub>2</sub> O <sub>3</sub>                        | 90.00         | 5.00   | -1.00                           | 2.48<br>(-1.40 V)                                  | [10]             |
| 8        | Bi <sub>2</sub> O <sub>3</sub>  | 98.00         | 22.00  | -1.00                           | 3.04<br>(-1.20 V)                                  | [11]             |
| 9        | f-Bi <sub>2</sub> O <sub>3</sub>  | 87.00         | 24.00  | -1.20                           | 3.98<br>(-1.20 V)                                  | [11]             |
| 10       | GaN/In <sub>2</sub> O <sub>3</sub> @P<br>CNF                            | 87.00         | 29.70  | -0.90                           | 4.95<br>(-1.20 V)                                  | [12]             |
| 11       | ER-HC   | 96.80         | 1.90   | -0.88                           | 2.36<br>(-0.98 V)                                  | [13]             |
| 12       | Bi/Cu foam  | 92.00         | 10.00  | -0.97                           | 2.98<br>(-1.17 V)                                  | [14]             |
| 13       | BiOx/C  | 93.40         | 18.00  | -1.00                           | 3.26<br>(-1.37 V)                                  | [15]             |
| 14       | Bi <sub>2</sub> S <sub>3</sub> -<br>Bi <sub>2</sub> O <sub>3</sub> @rGO | 90.00         | 6.14   | -0.90                           | 1.01<br>(-1.10 V)                                  | [16]             |
| 15       | Bi@NPC  | 92.00         | 14.4   | -0.87                           | 4.27<br>(-1.27 V)                                  | [17]             |
| 16       | Bi(1200)  | 97.5          | 5.50   | -0.87                           | 1.83<br>(-1.07 V)                                  | [18]             |
| 17       | Re-P  | 84.00         | 9.10   | -0.87                           | 3.99<br>(-1.17 V)                                  | [19]             |

**Table S2.** The summary of CO<sub>2</sub> electro-reduction performances of Cu/BMO NSs and other electrocatalysts in seawater.

|          | Catalyst                                    | Product         | FE (%)    | $j_{\text{HCOOH}}$ (mA cm <sup>-2</sup> ) | Stability (h) | Ref.             |
|----------|---|-----------------|-----------|---|---------------|------------------|
| <b>1</b> | <b>Cu/BMO NSs</b>                           | <b>HCOOH</b>    | <b>93</b> | <b>35.59</b>                              | <b>&gt;50</b> | <b>This work</b> |
| 2        | BDD   | HCHO            | 36        | -   | 20            | [20]             |
| 3        | CoPc/g-C <sub>3</sub> N <sub>4</sub>        | CO              | 89.5      | 16.00                                     | >2            | [21]             |
| 4        | N-Zn <sub>0.25</sub> Ni <sub>0.75</sub> O/C | CO              | 89        | 1.80                                      | -             | [22]             |
| 5        | Bi NPs                                      | HCOOH           | 81        | 47.00                                     | -             | [23]             |
| 6        | Polished Cu                                 | CH <sub>4</sub> | 5         | 5.00                                      | 4             | [24]             |
| 7        | Cu@ZIF-8C                                   | CO              | 94.3      | 30.00                                     | 1.5           | [25]             |

**Table S3.** The metal ions concentration in seawater before and after electrocatalysis for 10 h measured by ICP-MS.

| Seawater                    | Cu (ppm)     | Bi (ppm)     | Mo (ppm)     |
|-----------------------------|--------------|--------------|--------------|
| Natural seawater            | Not detected | Not detected | Not detected |
| After electrolysis for 10 h | 0.01         | 0.02         | 0.008        |

## Reference

1. J. P. Perdew, K. Burke and M. Ernzerhof, Generalized Gradient Approximation Made Simple, *Phys. Rev. Lett.*, 1996, **77**, 3865-3868.
2. G. Kresse and J. Furthmüller, Efficient iterative schemes for ab initio total-energy calculations using a plane-wave basis set, *Phys. rev. B.*, 1996, **54**, 11169.
3. J. K. Norskov, J. Rossmeisl, A. Logadottir, L. Lindqvist, J. R. Kitchin, T. Bligaard and H. Jonsson, Origin of the Overpotential for Oxygen Reduction at a Fuel-Cell Cathode, *J. Phys. Chem. B.*, 2004, **108**, 17886-17892.
4. A. A. Peterson, F. Abild-Pedersen, F. Studt, J. Rossmeisl and J. K. Norskov, How copper catalyzes the electroreduction of carbon dioxide into hydrocarbon fuels, *Energ. Environ. Sci.*, 2010, **3**, 1311-1315.
5. M. X. Wu, X. X. Zhang, Y. L. Xu, X. L. Cheng, W. C. Wang, N. Mitsuzaki, Z. Y. Ming and Z. D. Chen, Electrodeposition of Cu-Bi Alloys from a Non-Aqueous Solution for Electrochemical Reduction of CO<sub>2</sub>, *J. Electrochem. Soc.*, 2025, **172**, 032502.
6. B. Li, J. D. Chen, L. H. Wang, D. Xia, S. J. Mao, L. L. Xi, H. J. Liu, S. B. Ying and Y. Wang, High-Performance Bi-Based Catalysts for CO<sub>2</sub> Reduction: In Situ Formation of Bi/Bi<sub>2</sub>O<sub>2</sub>CO<sub>3</sub> and Enhanced Formate Production, *Adv. Sci.*, 2025, **12**, 2415616.
7. Z. Y. Yang, Y. X. Jin, X. S. Guan, Z. B. Feng, C. R. Feng, S. S. Li, P. F. Wang, X. W. An, Y. Duan, X. G. Hao, A. Abudula and G. Q. Guan, Tuning oxygen vacancy concentration in Indium oxide via sulfur doping for enhancing CO<sub>2</sub> electroreduction to formate, *Chem. Eng. J.*, 2025, **514**, 163049.
8. L. L. Zhou, Z. P. Qu, L. Fu and Y. Ding, Interfacial engineering of In-SnO<sub>2</sub> heterostructure for promoting electrocatalytic CO<sub>2</sub> reduction to formate, *Appl. Catal., B*, 2025, **377**, 163049.
9. Z. Wu, H. Wu, W. Cai, Z. Wen, B. Jia, L. Wang, W. Jin and T. Ma, Engineering Bismuth-Tin Interface in Bimetallic Aerogel with a 3D Porous Structure for Highly Selective Electrocatalytic CO<sub>2</sub> Reduction to HCOOH, *Angew. Chem., Int. Ed.*, 2021, **60**, 12554-12559.
10. J. Tian, R. Wang, M. Shen, X. Ma, H. Yao, Z. Hua and L. Zhang, Bi-Sn Oxides for Highly Selective CO<sub>2</sub> Electroreduction to Formate in a Wide Potential Window, *ChemSusChem*, 2021, **14**, 2247-2254.
11. T. Tran-Phu, R. Daiyan, Z. Fusco, Z. Ma, R. Amal and A. Tricoli, Nanostructured  $\beta$ -Bi<sub>2</sub>O<sub>3</sub> fractals on carbon fibers for highly selective CO<sub>2</sub> electroreduction to formate, *Adv. Funct. Mater.*, 2019, **30**, 1906478.
12. X. Li, X. Jiang, Y. Kong, J. Sun, Q. Hu, X. Chai, H. Yang and C. He, Interface engineering of a GaN/In<sub>2</sub>O<sub>3</sub> heterostructure for highly efficient electrocatalytic CO<sub>2</sub> reduction to formate, *Chinese J. Catal.*, 2023, **50**, 314-323.
13. D. Wang, S. Dong, L. Wen, W. Yu, Z. He, Q. Guo, X. Lu, L. Wang, S. Song and J. Ma, Highly selective electrocatalytic reduction of CO<sub>2</sub> to HCOOH over an in situ derived hydrocerussite thin film on a Pb substrate, *Chemosphere*, 2022, **291**, 132889.
14. X. An, S. Li, X. Hao, X. Du, T. Yu, Z. Wang, X. Hao, A. Abudula and G. Guan,

- The in situ morphology transformation of bismuth-based catalysts for the effective electroreduction of carbon dioxide, *Sustain. Energ. Fuels*, 2020, **4**, 2831-2840.
15. C. W. Lee, J. S. Hong, K. D. Yang, K. Jin, J. H. Lee, H.-Y. Ahn, H. Seo, N.-E. Sung and K. T. Nam, Selective electrochemical production of formate from carbon dioxide with bismuth-based catalysts in an aqueous electrolyte, *ACS Catal.*, 2018, **8**, 931-937.
  16. X. Yang, P. Deng, D. Liu, S. Zhao, D. Li, H. Wu, Y. Ma, B. Y. Xia, M. Li, C. Xiao and S. Ding, Partial sulfuration-induced defect and interface tailoring on bismuth oxide for promoting electrocatalytic CO<sub>2</sub> reduction, *J. Mater. Chem. A*, 2020, **8**, 2472-2480.
  17. D. Zhang, Z. Tao, F. Feng, B. He, W. Zhou, J. Sun, J. Xu, Q. Wang and L. Zhao, High efficiency and selectivity from synergy: Bi nanoparticles embedded in nitrogen doped porous carbon for electrochemical reduction of CO<sub>2</sub> to formate, *Electrochim. Acta.*, 2020, **334**, 135563.
  18. Y. Tian, D. Li, J. Wu, J. Liu, C. Li, G. Liu, D. Chen and Y. Feng, Electroreduction of CO<sub>2</sub> to formate with excellent selectivity and stability on nano-dendrite Bi film electrode, *J. CO<sub>2</sub> Util.*, 2021, **43**, 101360.
  19. J. Bei, R. Zhang, Z. Chen, W. Lv and W. Wang, Efficient Reduction of CO<sub>2</sub> to Formate Using in Situ Prepared Nano-Sized Bi Electrocatalyst, *Int. J. Electrochem. Sci.*, 2017, **12**, 2365-2375.
  20. K. Nakata, T. Ozaki, C. Terashima, A. Fujishima and Y. Einaga, High-yield electrochemical production of formaldehyde from CO<sub>2</sub> and seawater, *Angew. Chem., Int. Ed.*, 2014, **53**, 871-874.
  21. X. Tan, C. Yu, X. Song, C. Zhao, S. Cui, H. Xu, J. Chang, W. Guo, Z. Wang, Y. Xie and J. Qiu, Toward an understanding of the enhanced CO<sub>2</sub> electroreduction in NaCl electrolyte over CoPc molecule-implanted graphitic carbon nitride catalyst, *Adv. Energy Mater.*, 2021, **11**, 2100075.
  22. S. Zhang, X.-T. Gao, P.-F. Hou, T.-R. Zhang and P. Kang, Nitrogen-doped Zn–Ni oxide for electrochemical reduction of carbon dioxide in sea water, *Rare Metals*, 2021, **40**, 3117-3124.
  23. A. Mason, K. MacDonald, W. Murphy, C. Bennett and E. Bertin, Electroreduction of CO<sub>2</sub> on bismuth nanoparticles in seawater, *J. Appl. Electrochem.*, 2022, **53**, 217-226.
  24. S. Bai, M. Song, T. Ma, F. Wang, Y. Liu and L. Guo, On factors of ions in seawater for CO<sub>2</sub> reduction, *Appl. Catal., B* 2023, **323**, 122166.
  25. H. L. Hu, M. X. Han, H. Lin, J. H. Dai, K. X. Shen, M. Z. Li, X. C. Chen, A. Q. Zarifzoda, F. Z. Liu, Y. Chen and F. M. Chen, Fast Seawater Desalination Integrated with Electrochemical CO<sub>2</sub> Reduction, *Angew. Chem., Int. Ed.*, 2025, **64**, e202415806.